applied sciences

MDPI

Article

Assessment of the Impact of Orthodontic Miniscrew Insertion Angle on the Stress Distribution During Intrusion of Anterior Teeth: A 3D Finite Element Analysis

Salah Aldeen A. Alhgeg [1,*], R. Lale Taner [2,3], Orhan Özdiler [1] and K. Müfide Dinçer [1]

[1] Department of Orthodontics, Faculty of Dentistry, Cyprus Health and Social Sciences University, 99700 Mersin, Turkey; xyy56985@gmail.com (O.Ö.); mufidedincer@yahoo.com (K.M.D.)
[2] Department of Orthodontics, Faculty of Dentistry, Gazi University, 06490 Ankara, Turkey; laletaner@yahoo.com
[3] Department of Orthodontics, Faculty of Dentistry, Cyprus International University, 99258 Mersin, Turkey
* Correspondence: salahalhgeg1@gmail.com

Abstract

This study evaluated the biomechanically optimal insertion angle for miniscrew-assisted anterior intrusion by analyzing stress in the periodontal ligament (PDL) and alveolar bone. A three-dimensional finite element model from cone-beam computed tomography (CBCT) data, comprising maxillary bone, anterior dentition, and a bonded orthodontic appliance, and segmented 0.019 × 0.025-inch stainless-steel archwire were used. Titanium miniscrews (1.4 × 6 mm) were placed at 5 mm from the alveolar crest between the lateral incisor and canine. Four insertion angulations relative to the occlusal plane (30°, 60°, 90°, and 120°) were simulated under a 90 g intrusive force. Results demonstrated that while all configurations achieved intrusion with minor labial tipping and maintained miniscrew stability, stress localization was highly angle-dependent: the 90° insertion generated the highest central incisor PDL tensile stress and maximum cortical bone Von Mises stress; the 120° insertion yielded peak canine PDL Von Mises stress and maximum root displacement; and the 60° insertion localized peak stresses within the cancellous bone and the bone–implant interface. Miniscrews remained stable in all scenarios. While all tested miniscrew angulations provided stable anchorage for upper anterior teeth intrusion, the selection of insertion angle critically influenced stress patterns within the supporting tissues.

Keywords: temporary anchorage devices; titanium miniscrew; angle of the placement; anterior intrusion; biomechanical consideration; finite element analysis

Check for updates

Academic Editor: Gang Wei

Received: 21 January 2026
Revised: 6 February 2026
Accepted: 26 February 2026
Published: 2 March 2026

1. Introduction

Orthodontic movement, particularly intrusive displacement, is associated with an increased incidence of root resorption. The biomechanical basis for this risk lies in the distinct patterns of stress that different movements generate within the periodontium [1,2]. This risk is clinically relevant in the correction of a deep overbite, which necessitates a strategic selection between treatment modalities: posterior teeth extrusion, anterior teeth intrusion, or a combined approach. For patients exhibiting a significant interlabial gap accompanied by a gummy smile, the primary treatment strategy is the intrusion of the maxillary incisors [3–6].

The integration of temporary anchorage devices (TADs), specifically orthodontic miniscrews, has expanded the scope of achievable tooth movements, including those requiring absolute anchorage [7,8]. These devices offer clinically significant advantages: they tolerate immediate loading, involve a minimally invasive placement and removal protocol, provide multiple intraoral insertion sites with adequate bone density, and present a cost-effective treatment option [9,10]. For tooth intrusion, TADs are particularly indicated as they enable the application of controlled, light, and continuous forces. This approach eliminates reactive reciprocal forces on adjacent teeth and provides enhanced biomechanical control, which may reduce the incidence of associated apical root resorption [11–13]. Furthermore, it minimizes adverse sequelae such as labial tipping, a limitation frequently associated with conventional mechanics [14,15].

Primary implant stability in miniscrews is derived from mechanical interlocking and is influenced by factors including cortical bone density and thickness, surgical technique, and screw design [16,17]. The intentional placement of orthodontic miniscrews with a deliberate angulation to the cortical bone is a methodology supported in the literature. Its advantages are avoiding of adjacent root anatomy and optimizing the cortical bone-to-implant contact interface [18–22].

Accurately assessing the mechanical stress profiles within the complex periodontal environment and the biological changes they elicit remains technically challenging [23,24]. Given the ethical and practical constraints of in vivo studies, much existing biomechanical evidence derives from in vitro models, which are often limited by the use of non-human bone, destructive testing, and an inability to capture dynamic biological responses. Finite Element Analysis (FEA) serves as a vital computational bridge between theoretical biomechanics and clinical practice [25–28]. Finite Element Analysis (FEA) serves as a vital computational bridge between theoretical biomechanics and clinical practice. This technique permits the controlled simulation of various force systems and conditions, facilitating a quantitative assessment of force distribution without requiring additional patient or animal subjects [29–31].

While FEA studies have widely examined how miniscrew dimensions, thread design, and bone density affect mechanical stability [32,33], and systematic reviews have highlighted how insertion parameters influence success rates [34–37], the biomechanical effect of insertion angle continues to be discussed [38–40]. Since direct in vivo stress quantification is not clinically feasible, establishing a reliable FEA simulation model is a necessary step for understanding and mitigating the risks associated with intrusive tooth movement [1,2].

Therefore, this study utilizes 3D FEA to investigate the biomechanical effects of miniscrew insertion angle. The primary objective is to quantify its impact on stress distribution within the periodontal ligament and alveolar bone, assess the resulting displacement of the anterior teeth, and evaluate the mechanical stability of the miniscrew anchorage itself under a controlled intrusive orthodontic force.

2. Materials and Methods

2.1. Study Design

This investigation utilized three-dimensional (3D) finite element analysis (FEA) to evaluate the influence of miniscrew insertion angulation on stress distribution and the resultant displacement of maxillary anterior teeth during intrusion. The study specifically assessed miniscrew stability, stress patterns within the peri-implant bone and periodontal ligament (PDL), and the biomechanical response of the surrounding alveolar bone.

Titanium miniscrews (1.4 × 6 mm) were virtually placed 5 mm from the alveolar crest in the anterior maxilla [41]. Four insertion angulations (30°, 60°, 90°, and 120°) relative to the occlusal plane, were placed distal to the lateral incisors in both sides and were tested under a 90 g intrusive force applied perpendicular to the archwire using Niti closed coil (3M Unitek, formerly Unitek Corporation, Monrovia, CA, USA) [42,43].

The insertion point was determined by approximating the center of resistance (CRes) for the maxillary incisors. Based on anatomical reference, this point is estimated to be situated apically to an area between the distal root surface of the lateral incisor and the mesial root surface of the canine [44,45].

Four finite element models were created, each differentiated by the insertion angulation (30°, 60°, 90°, or 120°) of bilateral titanium miniscrews placed between the lateral incisors and canines. Each model featured anterior maxillary teeth with a segmented 0.019 × 0.025-inch stainless steel archwire from canine-to-canine, ligated to bonded orthodontic appliance (MBT) prescription brackets (0.022 × 0.028-inch) (3M Unitek Dental Products, Monrovia, CA, USA). Forces were applied perpendicular to this archwire in all simulations. Outcome measures included Von Mises stress (implant/bone), principal stresses (bone), and displacement vectors of the anterior teeth.

2.2. 3D Model Development

2.2.1. CBCT Imaging and Data Acquisition

A high-resolution CBCT scan (Figure 1) (voxel size: 0.25 mm; 120 kVp; 7 mA; FOV: 16 cm diameter, 4 cm height, and the total scanning time was 26.9 s) of a fully dentate maxilla was acquired to serve as the foundational dataset for generating a detailed 3D finite element model. The acquired volumetric data were exported in the standard Digital Imaging and Communications in Medicine (DICOM) format for further processing.

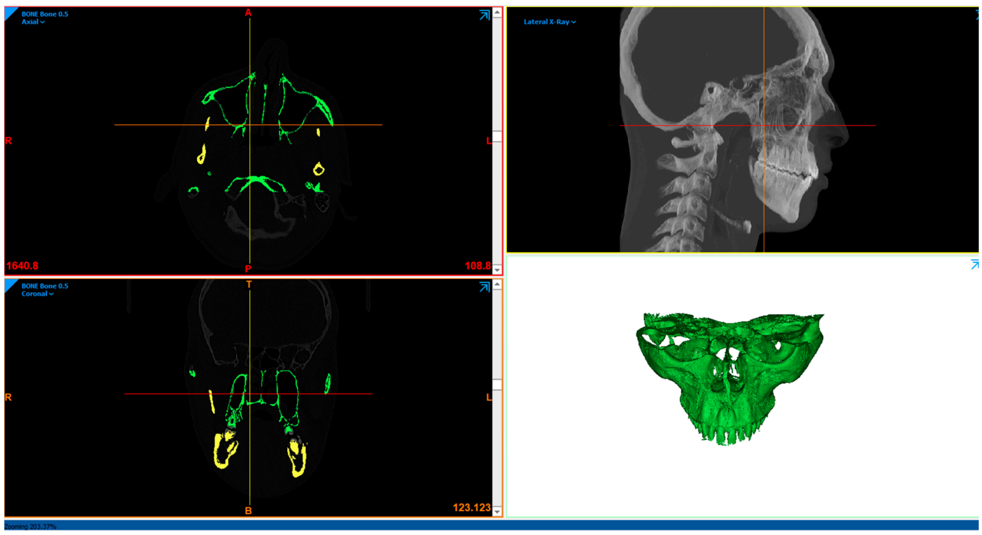

Figure 1. High-resolution CBCT scan of a fully dentate maxilla.

2.2.2. Segmentation and 3D Reconstruction

Segmentation and initial 3D reconstruction were performed using Mimics Research software 21.0 (Materialise NV, Leuven, Belgium) (Figure 2). The maxillary compact and cancellous bone compartments were delineated using threshold-based segmentation. Additionally, the anterior teeth within the defined region were digitally segmented to permit independent simulation of rotational displacement in later analytical stages. The derived surface models underwent processing in Geomagic Design X v2022 software (3D Systems, Rock Hill, SC, USA) for surface smoothing and refinement to enhance geometric fidelity.

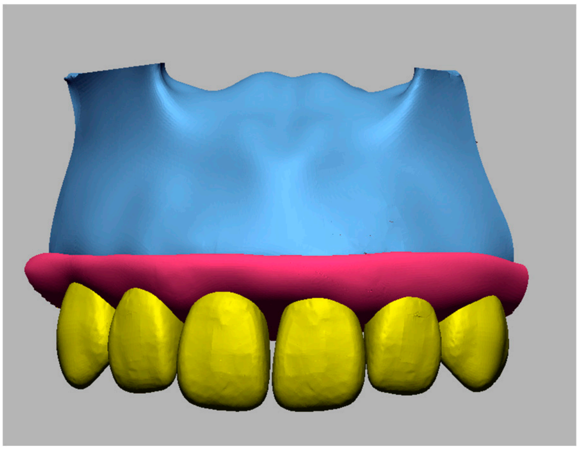

Figure 2. Segmentation and 3D reconstruction of individual anterior teeth.

2.2.3. Component Design and Reverse Engineering

The refined model of the maxillary bone and anterior teeth constituted the primary anatomical structure for the study. To complete the virtual assembly, necessary orthodontic components were designed digitally. All individual components were then prepared for final assembly within a computer-aided design environment.

2.2.4. Anterior Segment Model Assembly in SolidWorks

The complete 3D finite element assembly was constructed using SolidWorks software 2016 (SolidWorks Corp., Dassault Systèmes, Waltham, MA, USA). The assembly consisted of models for anterior maxillary teeth, brackets, a stainless steel archwire, and titanium miniscrews. The teeth were modeled with a surrounding periodontal ligament of constant 0.25 mm thickness [46]. The cortical bone was modeled with a thickness ranging from 1 mm at the alveolar crest to 2 mm at the apical region [47].

The appliance components were designed based on catalog specifications. MBT prescription brackets (0.022 × 0.028-inch) were positioned on the facial axis of each clinical crown. A 0.019 × 0.025-inch stainless steel archwire was modeled. Titanium miniscrews (Ti-6Al-4V, 1.4 × 6 mm) were modeled for insertion at 30°, 60°, 90°, and 120° angles. Boolean subtraction operations were performed to simulate the osteotomy for implant placement and to ensure correct alignment of all components within the bone.

2.3. Finite Element Analysis (FEA)

A three-dimensional FEA was done using ANSYS Transient Structural 2022 R2 software (ANSYS Inc., Canonsburg, PA, USA) to simulate the biomechanical effects of upper anterior teeth intrusion. The analysis comprised three sequential phases.

2.3.1. Pre-Processing and Meshing

The volumetric mesh was generated using 10-node tetrahedral elements (SOLID187). To ensure computational accuracy in regions of interest, a fine mesh with an approximate element size of 0.2 mm was applied to the teeth, PDL, and maxillary bone. The material properties (Table 1) and interface conditions were defined to replicate clinical behavior. The PDL-tooth interface was modeled as nonlinear viscoelastic to capture its elastic and plastic deformation during movement. The miniscrew-to-bone interfaces for titanium were modeled as rigid, simulating stable osseointegrated anchorage. Bracket-to-archwire contact was defined as frictional with a coefficient of 0.3. All other interfaces, including hooks, were modeled as perfectly bonded.

Table 1. Material properties and interface conditions applied to the finite element model.

Material	Modulus of Elasticity (GPa)	Poisson's Ratio
Compact bone [48]	13.7	0.30
Cancellous bone [49]	0.142	0.3
Miniscrew (Ti-6Al-4V:titanium-6%aluminium-4%vanadium) [50]	113.8	0.31
0.019 × 0.025″ stainless steel wire [51]	193.0	0.29
Periodontal ligament (PDL) [52]	0.07	0.45
Gingiva (soft tissue) [49]	0.0001	0.4
Preadjusted bracket (MBT slot 0.022″) [51]	197.0	0.29
NiTi closed coli spring [53]	48	0.3

2.3.2. Load Application and Boundary Conditions

For the simulation of upper anterior teeth intrusion, a bilateral titanium miniscrew anchorage system was modeled. The anterior maxillary segment was fully constrained in all directions to simulate clinical anchorage. Titanium miniscrews were positioned bilaterally between the lateral incisor and canine (Figure 3), and four distinct insertion angulations were evaluated: 30°, 60°, 90°, and 120°. In each configuration, forces were applied perpendicular to the archwire. The bone–miniscrew interface was defined as a frictional contact to replicate primary clinical stability, using a friction coefficient of 0.2 based on prior orthodontic finite element studies [54–56]. This formulation permitted limited relative displacement while preventing unrealistic interpenetration, thus better representing mechanical interlocking under initial loading. In each model, intrusion forces were applied perpendicular to the archwire to assess biomechanical response across the four angulations.

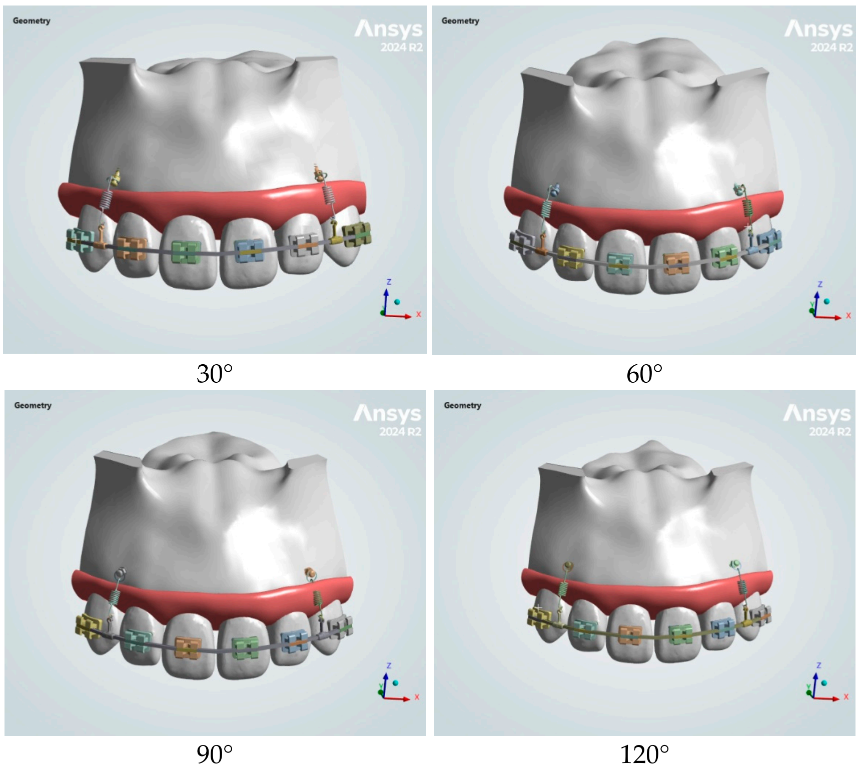

Figure 3. 3D assembly model with bilateral miniscrews placed at different insertion angle between the lateral incisor and canine.

2.3.3. Post-Processing and Outcome Measures

The post-processing phase evaluated the biomechanical response to orthodontic loading to comparatively assess the effects of miniscrew insertion angulation (30°, 60°, 90°, and 120°). For each model, the following primary outcome measures were extracted: Von Mises stress distribution within the titanium miniscrew; principal (compressive and tensile) stresses within the alveolar bone to identify regions at risk of remodeling; shear stress within the PDL as an indicator of potential tissue response; and the total deformation and three-dimensional (X, Y, Z) displacements of the miniscrew, PDL, dentin, and bone to quantify intrusive movement and anchorage stability.

2.4. Data Analysis

The extracted outcome measures were analyzed to determine the influence of insertion angulation on stress distribution and displacement patterns. The analysis specifically focused on: (1) stress concentration within the miniscrew body and at the bone-implant interface, (2) the propagation of stress to the periodontal ligament, and (3) the resulting magnitude and direction (intrusive vs. rotational) of anterior tooth displacement. Comparisons across angulation groups were performed to evaluate structural efficiency and mechanical integrity.

2.5. Model Validation

This finite element model was validated by comparing its simulated tooth displacement under intrusive loading with Mazhari et al. (2022) [57] which analyzed four different full-arch intrusion protocols using temporary skeletal anchorage.

Despite differences in experimental design including treatment extent (full-arch versus anterior segment intrusion), miniscrew configuration, and force application the present model demonstrated comparable qualitative trends in PDL hydrostatic pressure. Specifically, the central incisor exhibited the highest hydrostatic stress levels, followed by the lateral incisor and canine, consistent with the relative stress hierarchy reported by Mazhari et al. (2022) [57]. Their findings indicated that vertical intrusion was accompanied by coupled sagittal and transverse displacement components, reflecting a three-dimensional biomechanical response under intrusive loading.

A direct numerical comparison of displacement values is not appropriate due to significant methodological variations. However, the agreement in the qualitative mechanical behavior, specifically, the occurrence of intrusion with characteristic coupled movements supports the validity of the present model in replicating clinically realistic biomechanical responses. This approach of qualitative, pattern-based validation is well-accepted in finite element analysis, particularly when an identical reference model is unavailable [51,58].

Quantitative validation was not feasible due to methodological differences in geometry, material properties, loading conditions, and boundary constraints across published studies. Accordingly, validation was limited to qualitative comparison of biomechanical trends rather than direct numerical equivalence.

3. Results

3.1. Anterior Teeth Displacement

Displacement of the maxillary anterior teeth under a 90 g intrusive force delivered by a miniscrew was quantified using three-dimensional superimposition. The pre-load (blue) and post-load (green) digital models were compared to assess the movement of the central incisor, lateral incisor, and canine (Figure 4). Labial micromotion of the loaded teeth and an apical shift in the post-loaded structures were observed, confirming intrusive tooth movement. The directional displacement of the anterior teeth was assessed relative to the defined anatomical axes:

- X-axis: Distal (−)/Mesial (+);
- Y-axis: Palatal (+)/Labial (−);
- Z-axis: Intrusion (+)/Extrusion (−).

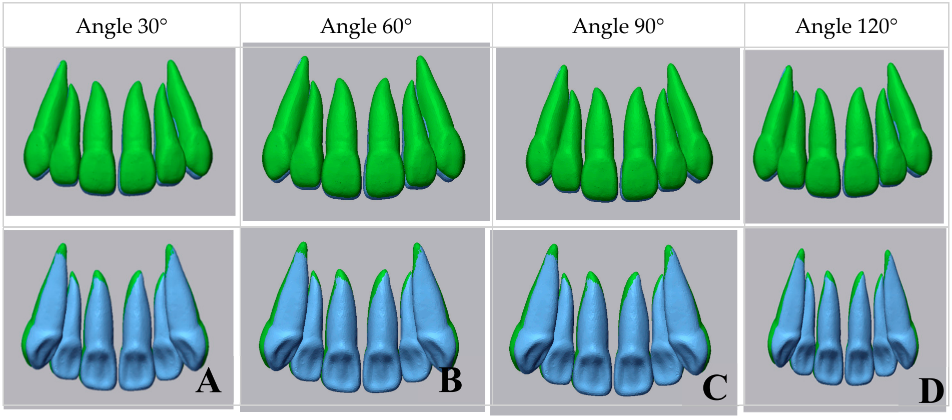

Figure 4. Superimposition of pre-load (blue) and post-load (green) models showing displacement vectors for intrusion at (**A**) 30°, (**B**) 60°, (**C**) 90°, and (**D**) 120° insertion angles.

The directional displacement of the anterior teeth was analyzed relative to a defined anatomical coordinate system, while the mechanical stress states of the teeth, periodontal ligament, and supporting bone were quantified under each loading condition. All tested insertion angles achieved intrusive movement in the anterior teeth, with vertical crown displacements of approximately 0.000101 mm for the central incisor and 0.000103 mm for the lateral incisor. The canine showed distinct patterns depending on the angle: at 30°, slight distal crown tipping and moderate intrusion; at 60°, maximum crown intrusion and the greatest mesial root movement; at 120°, pronounced vertical loading with strong mesial root displacement. Labial crown tipping and palatal root movement were consistent across all teeth, most notably in the lateral incisor, while mesiodistal movements remained negligible overall (Table 2 and Figure 5).

Table 2. Anatomical coordinate axes for displacement analysis (mm) under varied miniscrew insertion angles (30°, 60°, 90°, 120°).

Axis	Tooth	Angle 30°		Angle 60°		Angle 90°		Angle 120°	
Z-axis: Intrusion (+)/Extrusion (−) (mm)	Central incisal	Crown	Root	Crown	Root	Crown	Root	Crown	Root
		0.00010495	0.0000852	0.00010702	0.000087345	0.00010091	0.000081219	0.00010327	0.000083577
	Lateral incisal	Crown	Root	Crown	Root	Crown	Root	Crown	Root
		0.00010627	0.000089813	0.00010713	0.000091042	0.00010273	0.000086652	0.00010519	0.000093834
	Canine	Crown	Root	Crown	Root	Crown	Root	Crown	Root
		0.00011149	0.000089268	0.0001122	0.000090207	0.00011086	0.00008944	0.00011204	0.000090167
Y-axis: Palatal (+)/Labial (−) (mm)	Central incisal	Crown	Root	Crown	Root	Crown	Root	Crown	Root
		−0.000032287	0.0000052003	−0.000034256	0.0000045916	−0.000029136	0.0000052654	−0.000030524	0.0000049995
	Lateral incisal	Crown	Root	Crown	Root	Crown	Root	Crown	Root
		−0.000038155	0.0000008434	−0.000037659	0.0000008322	−0.000035001	0.0000010447	−0.000035943	0.0000020801
	Canine	Crown	Root	Crown	Root	Crown	Root	Crown	Root
		−0.000035638	0.0000079722	−0.000036166	0.0000085517	−0.000033755	0.0000083878	−0.000026916	0.0000086001

Table 2. *Cont.*

Axis	Tooth	Angle 30°		Angle 60°		Angle 90°		Angle 120°	
X-axis: Distal (−)/Mesial (+) (mm)	Central incisal	Crown	Root	Crown	Root	Crown	Root	Crown	Root
		0.0000023676	0.0000099844	−0.0000011138	0.0000092737	0.0000019389	0.000010378	0.0000010253	0.0000098004
	Lateral incisal	Crown	Root	Crown	Root	Crown	Root	Crown	Root
		−0.0000025918	0.000012588	−0.0000054945	0.000012679	−0.0000034397	0.000012753	−0.0000040328	0.000011071
	Canine	Crown	Root	Crown	Root	Crown	Root	Crown	Root
		−0.00001011	0.000015023	−0.000010554	0.000015308	−0.00001027	0.000015181	−0.000008551	0.000015236

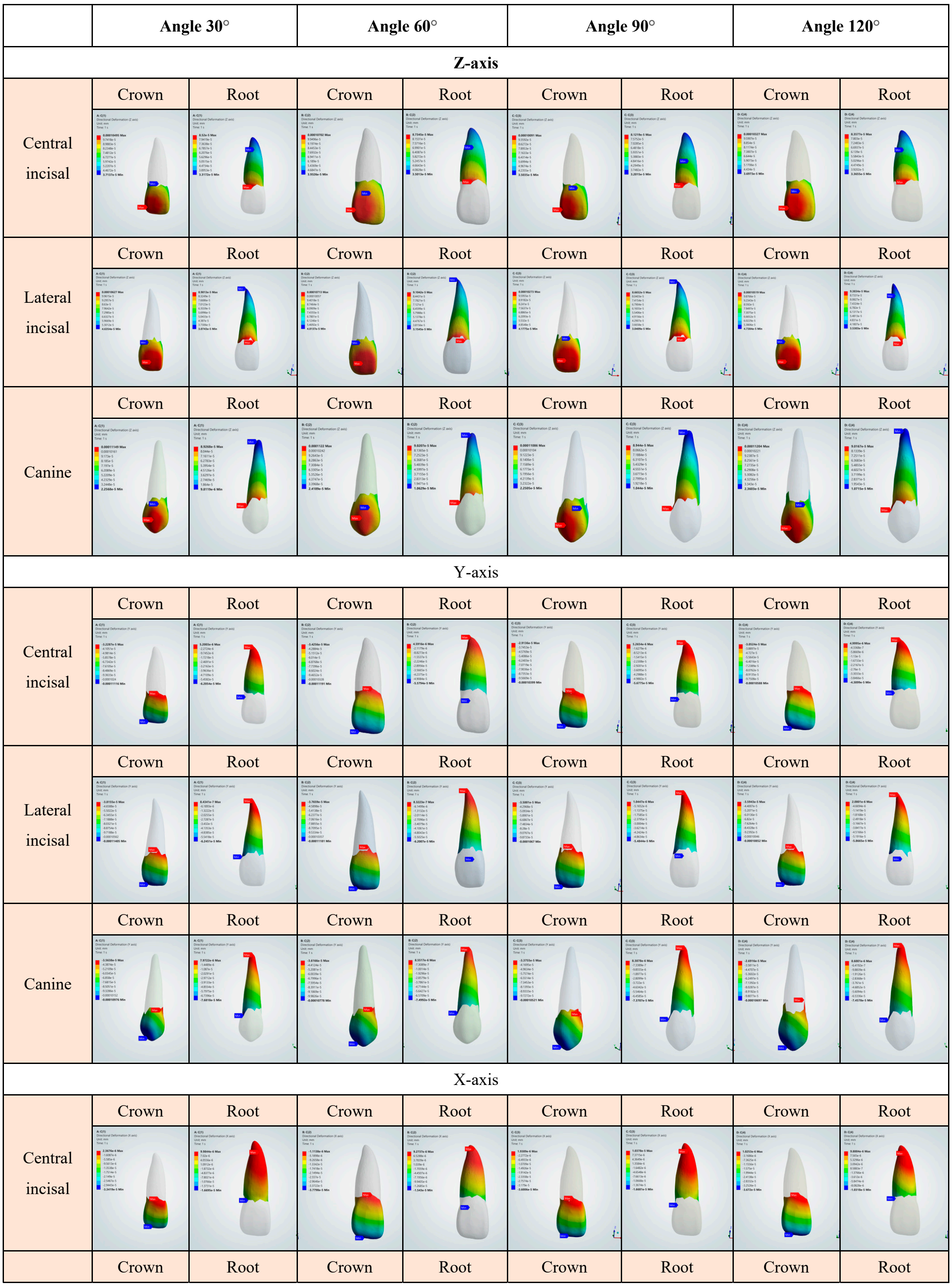

Figure 5. *Cont.*

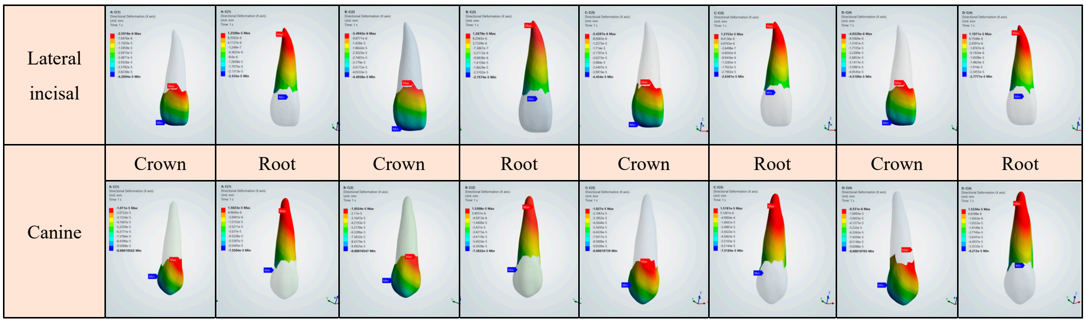

Figure 5. Anatomical coordinate axes for displacement analysis (mm) under varied miniscrew insertion angles.

3.2. Periodontal Ligament (PDL) Analysis

Stress distribution within the PDL was notably influenced by the miniscrew insertion angle, with a clear shift in the location of maximum stress as the angle increased (Table 3, Figures 6–8). The central incisor consistently exhibited a maximum principal stress (23.672 kPa) observed at the 90° angulation, while its Von Mises stress was also highest at 90° (27.058 kPa). In contrast, compressive stress within the central incisor PDL remained comparatively low across all models, ranging from 0.57136 to 0.62794 kPa.

The lateral incisor PDL demonstrated the lowest Von Mises stress. The minimum Von Mises stress value of 8.732 kPa was recorded at the 30° angulation. A distinct biomechanical response was noted at the 120° angulation, where the lateral incisor exhibited its maximum compressive stress of 1.8087 kPa, representing the highest compressive principal stress measured in the anterior segment.

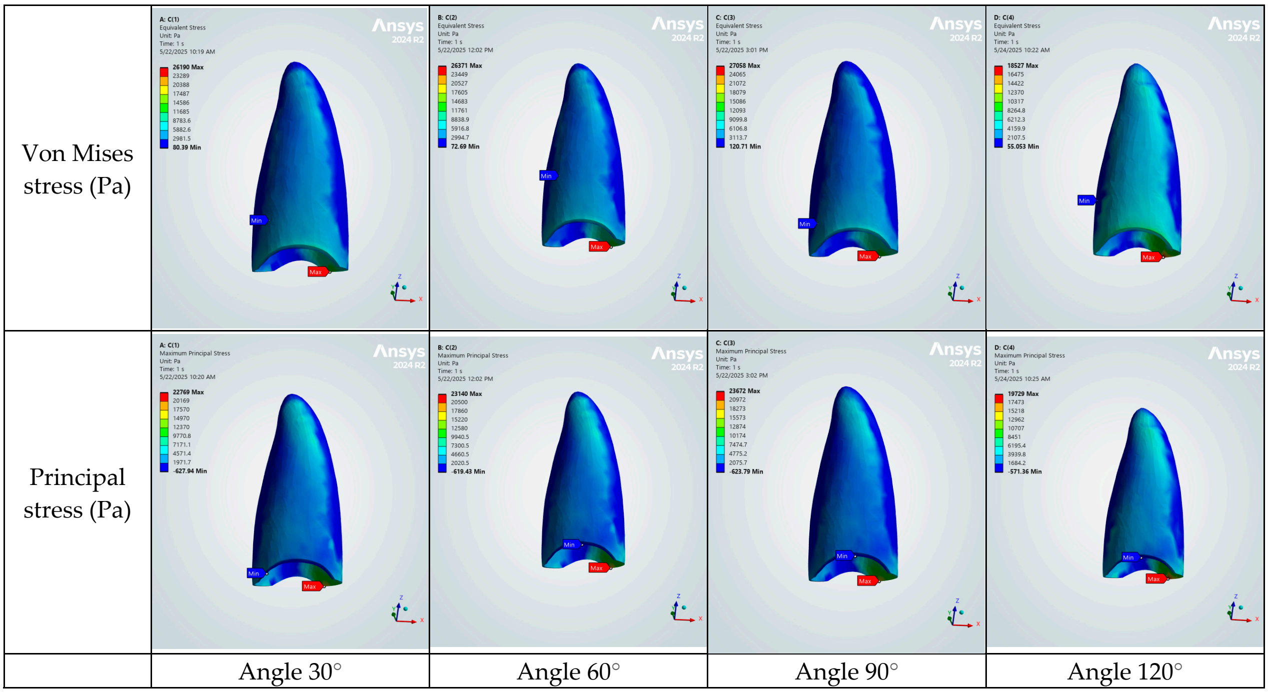

Figure 6. Distribution of Von Mises and principal stress within the PDL of the maxillary central incisor under different miniscrew insertion angles. Distribution of Von Mises stress (**top row**) and principal stress (**bottom row**) within the PDL under orthodontic intrusive force at four different angles.

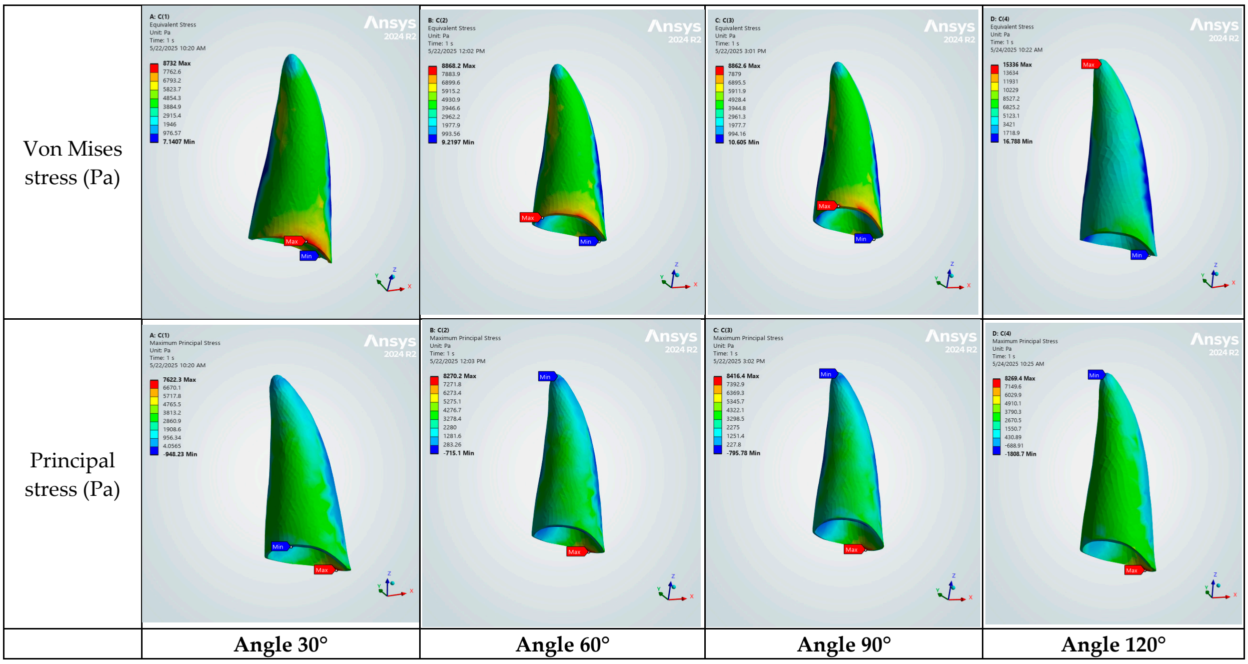

Figure 7. Distribution of Von Mises and principal stress within the PDL of the maxillary lateral incisor under different miniscrew insertion angle. Distribution of Von Mises stress (**top row**) and principal stress (**bottom row**) within the PDL under orthodontic intrusive force at four different angles.

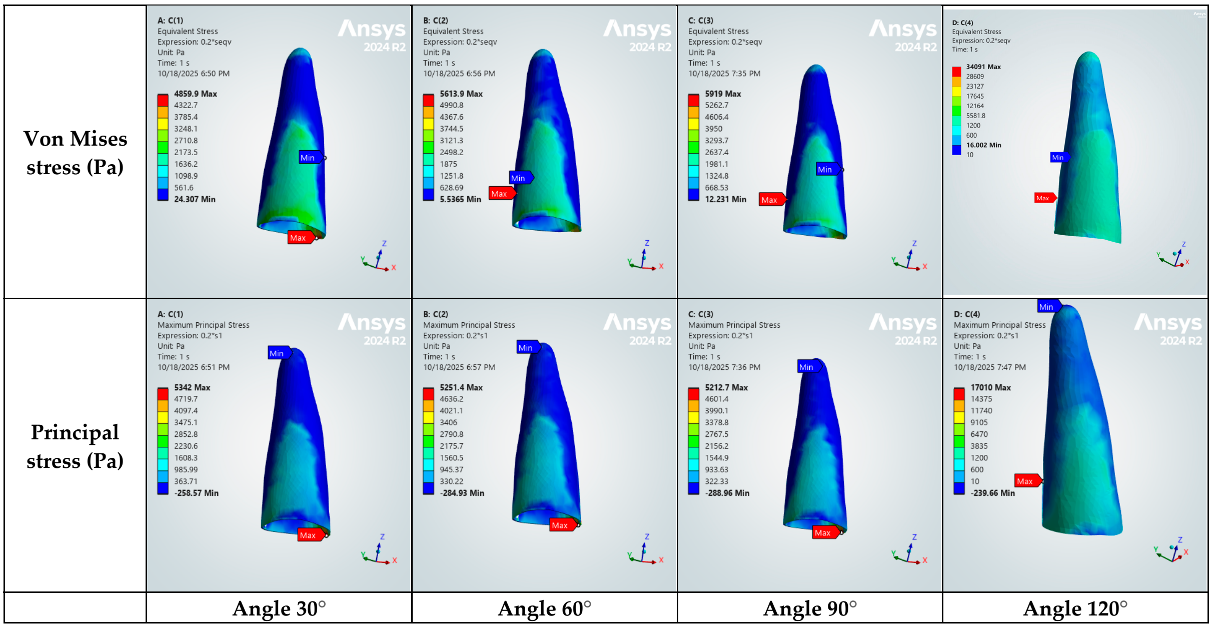

Figure 8. Distribution of Von Mises and principal stress within the PDL of the maxillary canine under different miniscrew insertion angles. Distribution of Von Mises stress (**top row**) and principal stress (**bottom row**) within the PDL under orthodontic intrusive force at four different angles.

The canine PDL presented the most pronounced variance in mechanical response. While typically demonstrating lower stress values, a substantial increase in Von Mises stress to 34.091 kPa was calculated at the 120° angulation, constituting the highest overall PDL stress recorded. At the same time, the canine exhibited the minimum principal stress values across the study: the lowest tensile stress was 5.2127 kPa at 90°, and the lowest compressive stress was 0.23966 kPa at the 120° angulation.

Table 3. Von Mises and maximum principal stress (kPa) in the periodontal ligament (PDL) under 30°, 60°, 90°, and 120° miniscrew insertion angles.

	Tooth	Angle 30°	Angle 60°	Angle 90°	Angle 120°
Von Mises stress	Central incisal	26.19	26.371	27.058	18.527
	Lateral incisal	8.732	8.8682	8.8626	15.336
	Canine	4.8599	5.6139	5.919	34.091
Principal stress (tensile)	Central incisal	22.769	23.14	23.672	19.729
	Lateral incisal	7.6223	8.2702	8.4164	8.2694
	Canine	5.342	5.2514	5.2127	17.01
Principal stress (compressive)	Central incisal	0.62794	0.61943	0.62379	0.57136
	Lateral incisal	0.94823	0.7151	0.79578	1.8087
	Canine	0.25857	0.28493	0.28896	0.23966

3.3. Bone Stress Analysis

3.3.1. Cortical Bone Stress Analysis

The cortical bone surrounding the central incisor demonstrated the greatest stress magnitudes for all angulation tested (Table 4). This region consistently showed the maximum Von Mises stress, which reached its highest level at 111.3 kPa under 90° loading, and the highest tensile principal stress, reaching 114.22 kPa. Compressive stresses in the central incisor's cortical bone were negligible by comparison. While the lateral incisor and canine demonstrated significantly lower stress levels, their patterns varied with angulation. Notably, the canine's Von Mises stress at the 30° insertion angle (89.449 kPa) was substantially higher than at the other angles (15.974–17.438 kPa), indicating a unique stress concentration for this specific configuration. These results confirm that the cortical bone near the central incisor root is the primary load-bearing structure during anterior intrusion, regardless of the miniscrew's insertion angle.

Table 4. Von Mises and principal stress (kPa) in the cortical bone surrounding the anterior teeth under intrusive orthodontic loading at 30°, 60°, 90°, and 120° insertion angles.

Stress Analysis	Tooth	Angle 30°	Angle 60°	Angle 90°	Angle 120°
Von Mises stress	Central incisal	105.64	110.89	111.3	101.05
	Lateral incisal	24.754	23.825	23.757	23.325
	Canine	89.449	17.438	15.974	16.867
Principal stress (tensile)	Central incisal	108.66	114.16	114.22	103.45
	Lateral incisal	24.633	24.021	24.017	23.607
	Canine	18.846	18.337	16.732	17.329
Principal stress (compressive)	Central incisal	0.69761	0.41425	0.4452	0.44409
	Lateral incisal	1.0695	1.0356	1.3833	0.26262
	Canine	0.20255	0.20255	0.14291	0.742

3.3.2. Cancellous Bone Stress Analysis

The stress within the cancellous bone showed a clear, angle-dependent pattern, with the central incisor region consistently experiencing the highest levels (Table 5). Under 90° loading, the central incisor's cancellous bone demonstrated a Von Mises stress of 20.778 kPa and a tensile stress of 21.042 kPa. The lateral incisor and canine exhibited significantly lower stress magnitudes. Stress distribution was notably sensitive to the insertion angle. The highest cancellous bone stress occurred at a 60° insertion, where the central incisor's

Von Mises stress reached 36.884 kPa. At the 120° angle, stress values generally decreased for the central and lateral incisors but increased for the canine, which showed its highest tensile stress (11.161 kPa) at this steep angulation. This indicates that the 60° configuration places the greatest biomechanical demand on the cancellous bone, while a 120° angle shifts a portion of the load distally toward the canine.

Table 5. Principal stress (KPa) and Von Mises stress (KPa) in the cancellous bone adjacent to the anterior teeth under intrusive force applied at different miniscrew insertion angles.

Stress Analysis	Tooth	Angle 30°	Angle 60°	Angle 90°	Angle 120°
Von Mises stress	Central incisal	30.027	36.884	20.778	11.417
	Lateral incisal	23.585	23.458	6.3823	12.286
	Canine	9.527	15.687	4.0614	7.8547
Principal stress (tensile)	Central incisal	27.925	34.433	21.042	9.8548
	Lateral incisal	17.623	16.863	4.9611	10.279
	Canine	5.3968	8.4328	3.9682	11.161
Principal stress (compressive)	Central incisal	1.2837	2.1856	0.7965	5.0289
	Lateral incisal	0.53493	1.763	0.24075	1.6153
	Canine	0.58285	0.5349	0.41394	0.48031

3.3.3. Peri-Implant Bone Analysis

At a 30° insertion angle, the cortical bone interface exhibited a maximum principal stress of 17.701 kPa, indicating a notable concentration of tensile force at the bone-implant contact zone. When the orthodontic loading angle was increased to 60°, the stress in the cortical bone increased substantially to a maximum of 30.888 kPa, demonstrating a significant localized tensile stress concentration. Under the same 60° loading, the adjacent cancellous bone experienced a markedly lower stress level, with a maximum principal stress of 0.74076 kPa (Table 6 and Figures 9 and 10).

Table 6. Maximum principal stress of peri-implant contact of cortical and cancellous bone with different miniscrew insertion angles.

Type of Analysis	Bone Type	Angle 30°	Angle 60°	Angle 90°	Angle 120°
Maximum principal stress of peri-implant contact (kPa)	Cortical bone	17.701	30.888	13.148	9.2173
	Cancellous bone	-	0.74076	2.298	1.0774

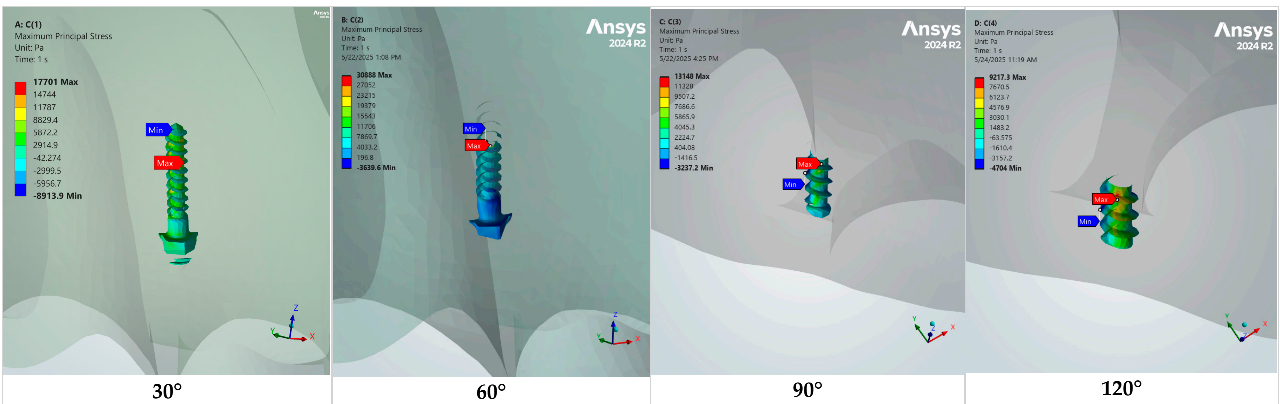

Figure 9. Finite element simulation illustrates the principal stress distribution on the peri-implant cortical bone surrounding the titanium miniscrew anchorage under intrusive orthodontic loading.

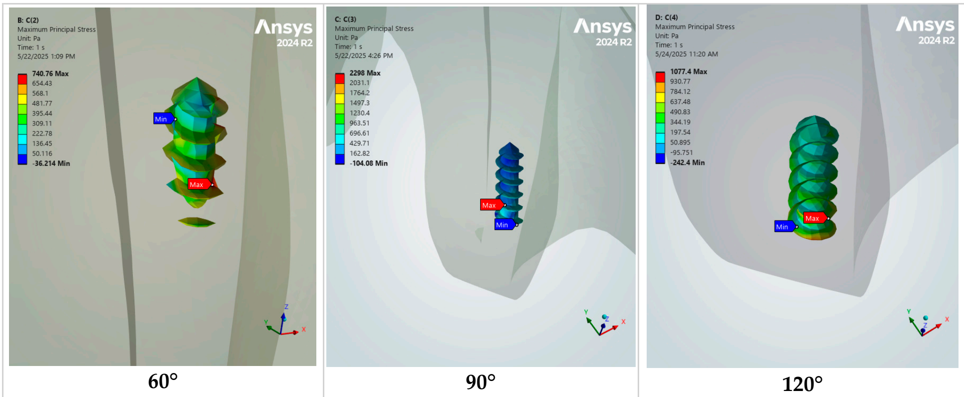

Figure 10. Finite element simulation illustrating the principal stress distribution on the peri-implant cancellous bone surrounding the titanium miniscrew anchorage under intrusive orthodontic loading.

Under a perpendicular 90° loading, the stress patterns were reduced. The cortical bone showed a maximum principal stress of 13.1 kPa, reflecting a controlled tensile load transfer. The cancellous bone, in contrast, demonstrated a mild tensile environment with a maximum principal stress of 2.3 kPa. At the maximum tested angle of 120°, the cortical bone interface experienced a maximum principal stress of 9.2173 kPa, while the cancellous bone presented a comparatively minor mechanical load, with a maximum principal stress of 1.0774 kPa (Table 6 and Figures 9 and 10).

3.4. Miniscrews Analysis

The titanium miniscrew, serving as anchorage between the roots of the maxillary lateral incisor and canine, demonstrated exceptional mechanical stability under all tested intrusive loading angles.

At a 30° insertion angle, the screw exhibited minimal deformation and stress, with a directional deformation of 0.000065 mm, a total displacement of 0.0000748 mm, and a maximum Von Mises stress of 3.006 kPa. These values indicate negligible movement and a very low risk of mechanical failure (Table 7 and Figure 11).

This pattern of high stability persisted across the other loading conditions. Under 60° loading, the directional deformation was approximately 0.0000682 mm, with a total displacement of approximately 0.0000769 mm and a maximum Von Mises stress of approximately 2.64 kPa. Similarly, at the 90° loading angle, the screw's performance was characterized by a directional deformation of approximately 0.0000672 mm, a total displacement of approximately 0.0000755 mm, and a Von Mises stress of approximately 2.29 kPa. The 120° loading condition resulted in a slightly higher but still minimal directional deformation of approximately 0.0000701 mm, a total displacement of approximately 0.0000770 mm, and a maximum Von Mises stress of approximately 6.27 kPa (Table 7 and Figure 11).

Table 7. Analysis of the titanium miniscrew with different miniscrew insertion angles.

Type of Analysis	Angle 30°	Angle 60°	Angle 90°	Angle 120°
Direction deformation (mm)	0.000065619	0.000068209	0.000067233	0.000070086
Total displacement (mm)	0.000074852	0.000076909	0.000075462	0.000077045
Maximum Von Mises stress (kPa)	3.0061	2.6415	2.286	6.2693

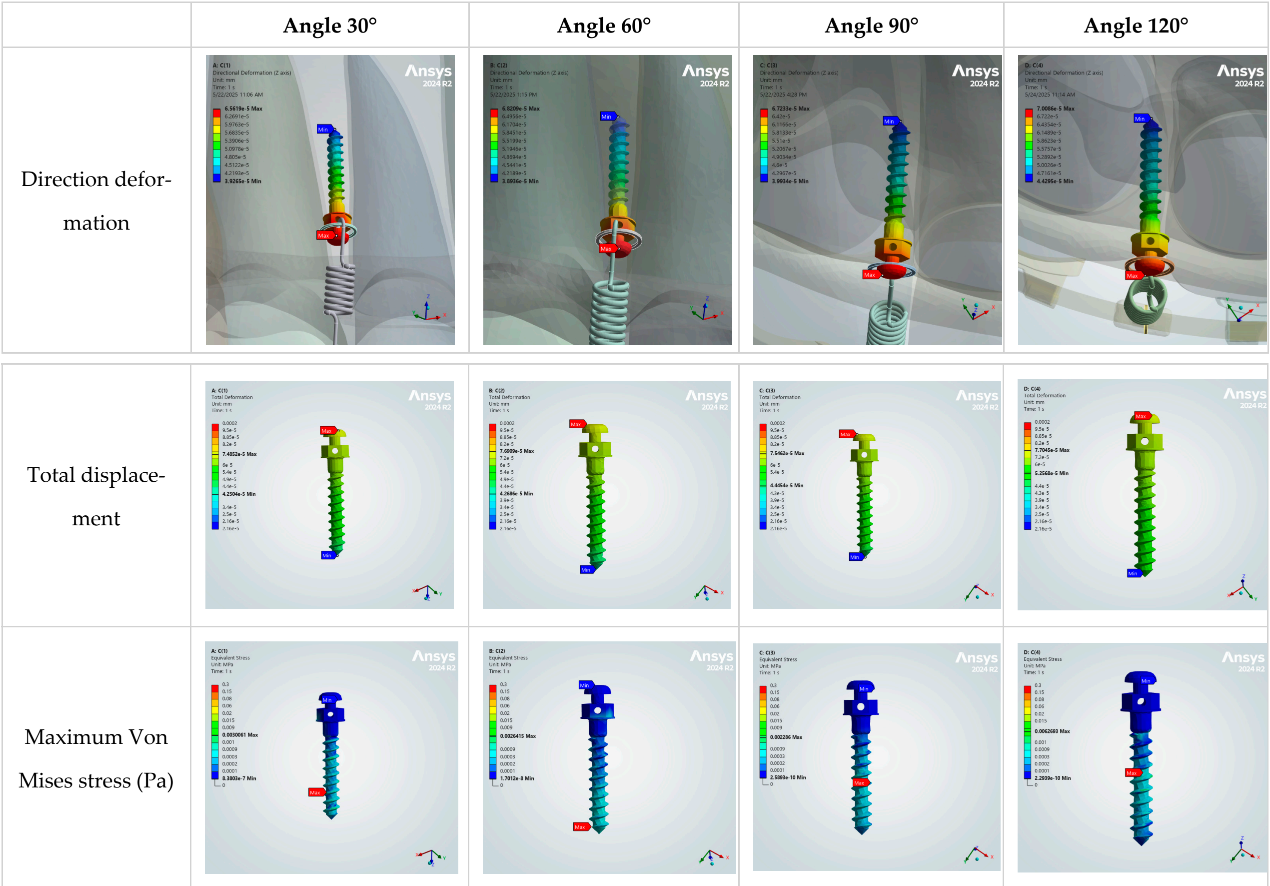

Figure 11. Representative finite element analysis results showing direction deformation, total displacement and maximum Von Mises stress of titanium miniscrews.

In all scenarios, the recorded deformations were negligible, with total displacements under 0.00008 mm, and the Von Mises stresses remained several orders of magnitude below the yield strength of titanium. This confirms the screw's role as a stable skeletal anchorage unit, with negligible positional change and no risk of material failure under the applied 90 g intrusive force (Table 7 and Figure 11).

4. Discussion

Finite element analysis (FEA) was employed to provide a detailed and reproducible assessment of orthodontic biomechanics under controlled conditions, thereby overcoming the inherent ethical and practical constraints of in vivo studies [17]. This computational approach effectively isolates the impact of miniscrew angulation by systematically manipulating the implant placement and force vector within identical, validated boundary conditions, which mitigates the confounding patient-specific variability in bone density and root anatomy present in clinical studies [59]. This methodological framework aligns with contemporary, validated orthodontic FEA research [60].

Material properties were assigned per established orthodontic FEA standards. Teeth, bone, and miniscrews were modeled as isotropic, linearly elastic solids, while the PDL was assigned nonlinear viscoelastic properties to simulate its time-dependent response, enhancing physiological relevance for comparative analysis [61]. The bone–implant interface was modeled as rigidly bonded to simulate primary mechanical stability under immediate orthodontic loading, a reliable assumption for stress transfer [62]. Contact interactions within the appliance system were defined to reflect clinical force transmission. A refined mesh of second-order tetrahedral elements was applied around the miniscrew neck, cortical bone, and PDL to capture steep stress gradients, a decisive strategy as insufficient refinement can underestimate peak stresses [40]. Virtual implant placement was achieved via Boolean subtraction across all test configurations [60].

The applied force magnitudes and directions reflected clinically accepted orthodontic loading. Anterior intrusive forces of 90 g were applied perpendicular to the archwire to simulate segmented intrusion mechanics. In multi-implant configurations, distributed forces created complex, single-vector loading, which is clinically relevant as force direction significantly affects stress propagation [63]. To ensure numerical stability and represent structural support, the posterior maxilla was constrained in all directions as the boundary condition, a simplified but widely accepted practice that does not distort comparative results when applied consistently [64].

The present finite element results provide a detailed biomechanical comparison of miniscrew-assisted anterior intrusion when the intrusive orthodontic load is applied with a different miniscrew insertion angle (30°, 60°, 90°, and 120°). By integrating tooth displacement (crown and root), PDL stress, alveolar bone stress (cortical and cancellous), peri-implant bone principal stress, and miniscrew deformation, the study offers a multi-tissue interpretation of how miniscrew angulation influences the intrusion of anterior teeth, an approach consistent with contemporary orthodontic FEM methodology [65].

Intrusion was reliably achieved across 30–120° in terms of displacement direction. Across all angles, the superimposition-based description (pre-load vs. post-load) indicating apical shift plus labial micromotion suggests that intrusion was achieved with a simultaneous labial component. This is biomechanically expected when the line of action does not pass exactly through the anterior segment's center of resistance. Even when the intent is intrusion, axial (vertical) force vectors tend to generate coupled moments that manifest as labial crown displacement and compensatory root movements. Quantitatively, the anterior teeth exhibited minimal absolute displacement, with crown intrusion measuring approximately 0.000101 mm for the central incisor and 0.000103 mm for the lateral incisor, reflecting "initial" elastic deformation rather than clinical displacement, which is typical for linear-elastic FEM simulations of orthodontic loading. These magnitudes should be interpreted as comparative indicators (between angles and teeth) rather than literal predictions of daily movement rates [65].

A consistent finding across 30°, 60°, 90°, and 120° was that crown intrusion along the Z-axis remained within a narrow range among the anterior teeth, whereas the labiolingual component (Y-axis) varied according to screw angulation and tooth type. This pattern suggests that altering screw angulation primarily redistributes the non-vertical component, influencing tipping tendencies, rather than substantially changing the magnitude of vertical intrusion itself. Thus, screw angulation mainly modulates the side effects of the applied load rather than determining whether intrusion occurs [66]. The crown–root displacement asymmetry seen particularly in the lateral incisor (distal crown shift with mesial root shift in several conditions) is characteristic of rotational movement about a resistance center rather than bodily translation. Clinically, this matters because intrusion combined with uncontrolled tipping may increase localized PDL stress and influence the risk profile for adverse effects (e.g., external apical root resorption) when maintained over time [67].

The PDL analysis highlighted that tissue-level stress distribution is more sensitive to angulation than the gross intrusion magnitude: At 30°, 60°, and 90°, the central incisor consistently demonstrated the highest PDL Von Mises stress (26.000 kPa to 27.000 kPa) and tensile principal stress (23 kPa), indicating that it acted as the primary stress-bearing unit within the anterior segment under those loading vectors. At 120°, the pattern shifted markedly: canine PDL Von Mises stress increased substantially (34.1 kPa), and lateral incisor PDL stresses increased as well, while central incisor PDL stress decreased compared with the 30–90° range. This redistribution implies that higher angulation may redirect force transmission toward the canine unit and its supporting tissues, which is clinically relevant because the canine region frequently becomes a key anchor/tooth movement mediator in anterior biomechanics. Comparable findings, where altered force direction changes which tooth/PDL regions experience peak stresses have been described in FEA studies evaluating miniscrew-assisted anterior mechanics [68].

The magnitude of PDL stress observed in the present study falls within the commonly reported orthodontic physiological range (approximately 20–260 kPa) [69,70], which is generally associated with controlled tooth movement without pathological root resorption. Excessive compressive stresses exceeding capillary blood pressure thresholds (~4.7 kPa) may impair vascular perfusion [39]; however, localized peak stresses in finite element models do not necessarily indicate sustained biological overload.

Bone stress results demonstrated two clinically important patterns. First, cortical bone surrounding the central incisor consistently acted as the dominant stress concentration region across all insertion angles, exhibiting high Von Mises and maximum tensile principal stresses (101.0–111.0 kPa). This indicates that irrespective of insertion angle, load transfer from the appliance was preferentially routed through the anterior cortical envelope in the central incisor region. Second, cancellous bone stresses exhibited a nonlinear dependence on insertion angle: cancellous stress around the central incisor peaked at 60° (Von Mises: 36.9 kPa) and decreased at 90°, with a further reduction at 120°. This behavior reflects the sensitivity of trabecular bone to insertion angle–dependent load orientation and boundary conditions, rather than a simple monotonic increase with increasing obliquity. Accordingly, variations in insertion angle primarily altered how stresses were distributed within the cancellous compartment rather than uniformly amplifying stress magnitude [10,63].

Among the evaluated insertion angles, the 60° configuration produced the highest maximum principal stress at the peri-implant bone interface, indicating a more mechanically demanding condition for the surrounding bone in this model. This elevated stress level is likely attributable to increased bending moments and shear stress components generated by oblique force transfer at this inclination, particularly near the cortical bone region. This finding aligns with recent FEA evidence showing that insertion angle and force direction interact strongly to determine cortical stress concentration around miniscrews, and that certain angulations can amplify bone-interface stress even when overall screw deformation remains minimal [65,71].

The finding that placing the microimplant at a 30-degree angle created more stress in the bone than placing it at 90 degrees matches the results from Jasmine et al. (2012) [72]. In a clinical setting, this higher stress could attract more cytokines, macrophages, and other inflammatory substances to the area. This increased activity might raise the risk of the microimplant becoming loose and failing. Most failures of dental implants are linked to too much stress and strain at the point where the implant meets the bone, which causes inflammation and can lead to bone loss around the miniscrews [73].

Despite angle-dependent changes at the interface, the miniscrew itself exhibited negligible deformation and displacement across all cases (directional deformation: 0.000065–0.000070 mm; total displacement (0.000075–0.000077 mm) and very low Von Mises stress (0.0023–0.0063 kPa). This indicates that within the tested load magnitude and boundary conditions, the miniscrew operated well within safe mechanical limits, and the dominant biomechanical concern becomes interface stress distribution (bone response) rather than screw material failure consistent with contemporary miniscrew FEA and related biomechanical studies [74].

Although the study focuses on orthodontic tooth movement rather than implant osseointegration, micromotion concepts remain useful to contextualize whether computed interface displacements are mechanically "small." A recent systematic review assessing tolerable micromotion emphasized that a single universal threshold is difficult to define across models and conditions, but excessive micromotion is repeatedly associated with impaired bone healing and fibrous encapsulation in many experimental contexts [75,76]. In the models, displacements at the miniscrew were far below commonly discussed high-risk magnitudes, supporting stable anchorage under the simulated conditions.

Intrusion was reliably achieved across 30–120° in terms of displacement direction. 120° shifted periodontal burden toward the canine, which may increase periodontal loading demand in that unit and should be considered when planning force vectors for controlled anterior intrusion. Among the tested configurations, the 60° insertion angle generated the highest maximum principal stress at the peri-implant bone interface. This finding indicates a more mechanically demanding bone–miniscrew interaction, likely resulting from increased oblique load components and bending moments at the cortical bone entry region. While such stress concentrations do not imply mechanical risk to the miniscrew itself, they reflect enhanced load transfer and anchorage engagement under the given anatomical and boundary conditions. Consequently, the 60° configuration may be considered mechanically effective for force delivery, although its higher biological demand underscores the need for cautious interpretation rather than designation as an optimal insertion angle.

It is important to clarify that the displacement values reported in this study (on the order of ~0.0001 mm) represent the initial elastic deformation of the tooth–periodontal ligament–bone complex under static, instantaneous loading, rather than true clinical orthodontic tooth movement. As in the majority of orthodontic finite element studies, the applied force was modeled as a static load to evaluate the immediate mechanical response of the system, not the time-dependent biological process of tooth movement. Under linear-elastic material assumptions and static loading conditions, micrometer-scale displacements reflect the immediate structural deformation occurring prior to periodontal ligament remodeling and alveolar bone adaptation. Displacement magnitudes of this order are widely reported in comparable orthodontic FEA studies and are considered appropriate for relative biomechanical comparison. Accordingly, the displacement results in the present study should be interpreted as comparative indicators of force transmission and stress redistribution between different miniscrew insertion angles, rather than predictors of the magnitude or rate of clinical tooth movement.

Consequently, clinicians are advised to avoid a 120° angulation in cases with pre-existing canine periodontal concerns. In contrast, a 60° insertion angle demonstrated higher peri-implant principal stress, reflecting enhanced load transfer and anchorage engagement at the bone–miniscrew interface. While this mechanical behavior may be advantageous in terms of stability and force transmission when adequate cortical bone thickness is present, it also indicates a greater biological demand on the surrounding bone. Therefore, the 60° angulation should be applied judiciously in regions with thin cortical bone, balancing its mechanical effectiveness against potential biological limitations.

The findings from this study offer several key insights for orthodontists using miniscrew-assisted mechanics for maxillary anterior intrusion. While all tested insertion angles (30°, 60°, 90°, and 120°) successfully achieved intrusive displacement under a 90 g force, the biomechanical response of the PDL, alveolar bone, and peri-implant interface varied significantly depending on the angulation. Clinically, this indicates that intrusion efficiency is relatively stable across different angles, but the choice of angulation is a critical tool for managing unwanted tipping and stress distribution. For instance, at 30°, 60°, and 90°, the central incisor serves as the primary stress-bearing unit; however, at 120°, the stress burden shifts toward the canine. This shift suggests that steeper insertion angles may increase the risk of adverse responses, such as root resorption or attachment loss, in patients with compromised canine periodontal support.

Furthermore, the cortical bone surrounding the central incisors remains the principal load-bearing structure, but the stress within the cancellous bone and the peri-implant interface peaks at a 60° insertion angle. This indicates that while a 60° angle may enhance anchorage engagement and load transfer, it also imposes a higher biological demand on the surrounding bone, requiring careful evaluation of cortical bone thickness and density before application. In practice, 30–90° angulations provide a stable, centralized stress distribution suitable for routine cases, whereas a 60° angle may be used to maximize anchorage in dense bone. Conversely, a 120° angle should be used with caution to avoid overloading the canines. Ultimately, clinicians must balance mechanical effectiveness with biological tolerance, selecting the insertion angle that best protects the patient's specific periodontal and bone anatomy.

Despite the insights gained from this finite element analysis, several inherent limitations must be considered. The PDL and bone tissues were modeled with idealized, homogeneous, linear elastic properties; however, in vivo, these tissues exhibit anisotropy, viscoelasticity, and nonlinear behavior that significantly alter stress–strain responses, particularly under long-term loading. Furthermore, the model was derived from the anatomy of a single patient, which limits the generalizability of the results to individuals with varying bone densities and root morphologies. Boundary conditions were simplified by fully constraining the maxillary bone to simulate anchorage, failing to capture the physiological compliance of the craniofacial complex or the force distribution effects of adjacent teeth. The assumption of a perfectly rigid miniscrew–bone interface also neglects the impact of micro-motion, cortical bone perforation angles, and insertion torque variations. Additionally, while a 90 g intrusive force was applied in a quasi-static model, biological tooth movement is a time-dependent process involving bone remodeling and PDL adaptation that cannot be fully captured by linear static FEA. This focus on a single force magnitude and direction also overlooks the potential effects of asymmetrical loading. Because finite element models only approximate biological processes, these findings regarding root resorption risk and miniscrew stability must be validated with longitudinal clinical studies. Future research should employ patient-specific, nonlinear viscoelastic models and dynamic loading schemes to better incorporate biological thresholds and improve predictive clinical accuracy.

5. Conclusions

Within the limitations of this three-dimensional finite element analysis, miniscrew insertion angulation significantly influenced stress distribution within the periodontal ligament, alveolar bone, and peri-implant interface during maxillary anterior intrusion, while having a minimal effect on the magnitude of vertical intrusive displacement. All tested angulations (30°, 60°, 90°, and 120°) produced effective intrusion under a 90 g force and demonstrated excellent mechanical stability, with negligible miniscrew deformation and stresses well below material failure thresholds.

Despite comparable intrusion efficiency, insertion angles markedly altered biomechanical stress patterns. A 90° angulation concentrated tensile stresses in the periodontal ligament and cortical bone of the central incisor. A 120° angulation shifted stress toward the canine, resulting in the highest periodontal ligament stress and increased canine root displacement. Conversely, a 60° angulation resulted in the greatest stress concentration at the peri-implant cortical interface and within the surrounding cancellous bone, reflecting an increased biomechanical demand on the anchorage site, despite the miniscrew remaining mechanically stable under the applied loading conditions.

Clinically, these findings highlight that miniscrew angulation primarily governs stress redistribution and potential side effects rather than intrusion effectiveness. Steep angulations should be used cautiously in patients with compromised canine periodontal support, while oblique angulations require sufficient cortical bone thickness to reduce peri-implant stress. In the planning of anterior intrusion mechanics, finite element analysis maintains its relevance as a key tool for the biomechanical optimization of miniscrews and the advancement of evidence-based clinical strategies.

Author Contributions: Conceptualization, S.A.A.A. and K.M.D.; methodology, O.Ö.; validation, S.A.A.A. and R.L.T.; formal analysis, S.A.A.A.; investigation, R.L.T.; resources, O.Ö.; data curation, S.A.A.A. and O.Ö.; writing—original draft preparation, S.A.A.A.; writing—review and editing, R.L.T. and K.M.D.; visualization, O.Ö.; supervision, K.M.D.; project administration, R.L.T. All authors have read and agreed to the published version of the manuscript.

Funding: This research received no external funding.

Institutional Review Board Statement: Ethical approval for this FEA study was approved by the Scientific Research Ethics Committee of the Cyprus Health and Social Sciences University (Approval Code: KSTU//2024/357) on 15 January 2025.

Informed Consent Statement: Informed consent was obtained from all subjects involved in the study.

Data Availability Statement: The data that support the findings of this study are available on request from the corresponding author.

Acknowledgments: The authors would like to thank Mohamed Gamal Askar for his technical assistance in the finite element analysis. The simulations were performed on a contractual basis, and his contribution during the modeling stage is sincerely appreciated.

Conflicts of Interest: The authors declare no conflicts of interest.

Abbreviations

The following abbreviations are used in this manuscript:

PDL	Periodontal ligament
CBCT	Cone-beam computed tomography
TADs	Temporary anchorage devices
FEA	Finite element analysis
3D	Three-dimensional
CRes	Center of resistance
DICOM	Digital Imaging and Communications in Medicine

References

1. Rudolph, D.J.; Sameshima, G.T. A finite element model of apical force distribution from orthodontic tooth movement. *Angle Orthod.* **2001**, *71*, 127–131.
2. Viglianisi, G.; Polizzi, A.; Lombardi, T.; Amato, M.; Grippaudo, C.; Isola, G. Biomechanical and Biological Multidisciplinary Strategies in the Orthodontic Treatment of Patients with Periodontal Diseases: A Review of the Literature. *Bioengineering* **2025**, *12*, 49. [CrossRef]
3. Burstone, C.R. Deep overbite correction by intrusion. *Am. J. Orthod.* **1977**, *72*, 1–22. [CrossRef]
4. Ansong, M.G.M. *Treatment of Increase Overbite in a Non Growing Patient (Final Degree Project)*; Universidad Europea: Madrid, Spain, 2023.
5. Akdaş, E.K. Gummy Smile Etiology and Treatment Options. *Selcuk. Dent. J.* **2025**, *12*, 166–171. [CrossRef]
6. Inchingolo, A.D.; Inchingolo, A.M.; Viapiano, F.; Netti, A.; Ciocia, A.M.; Ferrara, I.; Mancini, A.; Palermo, A.; Inchingolo, F.; Dipalma, G. Effectiveness and personalized approaches in the correction of gummy smile: A systematic review of orthodontic and surgical treatments. *J. Clin. Med.* **2024**, *13*, 6843. [CrossRef]
7. Bungau, T.C.; Marin, R.C.; Țenț, A.; Ciavoi, G. Temporary Anchorage Devices in Orthodontics: A Narrative Review of Biomechanical Foundations, Clinical Protocols, and Technological Advances. *Appl. Sci.* **2025**, *15*, 13035. [CrossRef]

8. Ritchie, C.; McGregor, S.; Bearn, D.R. Temporary anchorage devices and the forces and effects on the dentition and surrounding structures during orthodontic treatment: A scoping review. *Eur. J. Orthod.* **2023**, *45*, 324–337. [CrossRef]
9. Renna, G.; Leo, P.; Laurenziello, M.; Ciavarella, D. Overview of Mini-screws in Orthodontics. In *International Workshop on Engineering Methodologies for Medicine and Sport*; Springer: Berlin/Heidelberg, Germany, 2024; pp. 12–28.
10. Umalkar, S.S.; Jadhav, V.V.; Paul, P.; Reche, A. Modern anchorage systems in orthodontics. *Cureus* **2022**, *14*, e31476. [CrossRef] [PubMed]
11. Ohnishi, H.; Yagi, T.; Yasuda, Y.; Takada, K. A mini-implant for orthodontic anchorage in a deep overbite case. *Angle Orthod.* **2005**, *75*, 444–452. [CrossRef] [PubMed]
12. Polat-Ozsoy, O.; Arman-Ozcirpici, A.; Veziroglu, F. Miniscrews for upper incisor intrusion. *Eur. J. Orthod.* **2009**, *31*, 412–416. [CrossRef]
13. Baxi, S.; Bhatia, V.; Tripathi, A.; Dubey, M.P.; Kumar, P.; Mapare, S. Temporary Anchorage Devices. *Cureus* **2023**, *15*, e44514. [CrossRef]
14. Gupta, H.; Gupta, A.; Verma, S.; Singh, S.P. Comparing the Effect of Miniscrew-Supported and Conventional Maxillary Incisor Intrusion on the Inclination of Maxillary Incisors and Molars—A Systematic Review and Meta-Analysis. *Contemp. Clin. Dent.* **2022**, *13*, 307–314. [CrossRef]
15. Uzunçibuk, H. Assessment of the Mechanical Methods Employed in Incisor Intrusion During Orthodontic Treatment-A Narrative Literature. In *Studies in Dentistry*; Serüven Yayınevi: Ankara, Turkey, 2024; pp. 1–19.
16. Miyawaki, S.; Koyama, I.; Inoue, M.; Mishima, K.; Sugahara, T.; Takano-Yamamoto, T. Factors associated with the stability of titanium screws placed in the posterior region for orthodontic anchorage. *Am. J. Orthod. Dentofac. Orthop.* **2003**, *124*, 373–378. [CrossRef]
17. Toala, C.M. Stability of mini implants in the periodontum during orthodontic treatment. *Medicon. Dent. Sci.* **2024**, *4*, 2–10. [CrossRef]
18. Wilmes, B.; Drescher, D. Impact of insertion depth and predrilling diameter on primary stability of orthodontic mini-implants. *Angle Orthod.* **2009**, *79*, 609–614. [CrossRef]
19. Carano, A.; Velo, S.; Leone, P.; Siciliani, G. Clinical applications of the miniscrew anchorage system. *J. Clin. Orthod.* **2005**, *39*, 9–24. [PubMed]
20. Deguchi, T.; Nasu, M.; Murakami, K.; Yabuuchi, T.; Kamioka, H.; Takano-Yamamoto, T. Quantitative evaluation of cortical bone thickness with computed tomographic scanning for orthodontic implants. *Am. J. Orthod. Dentofac. Orthop.* **2006**, *129*, 721.e7–721.e12. [CrossRef]
21. Verma, S.K.; G, A.; Yadav, P.K.; M.P, A.A.; Brij, D. Enhancing orthodontic precision: A comprehensive review of temporary anchorage devices. *J. Dent. Panacea* **2024**, *6*, 92–102. [CrossRef]
22. del Rosso, C.; Poli, P.P.; Ghizzoni, M.; Caprioglio, A. Clinical Management of Orthodontic Miniscrew Complications: A Scoping Review. *Dent. J.* **2025**, *13*, 582. [CrossRef] [PubMed]
23. Tanne, K.; Sakuda, M.; Burstone, C.J. Three-dimensional finite element analysis for stress in the periodontal tissue by orthodontic forces. *Am. J. Orthod. Dentofac. Orthop.* **1987**, *92*, 499–505. [CrossRef]
24. Ovy, E.G.; Romanyk, D.L.; Mir, C.F.; Westover, L. Modelling and evaluating periodontal ligament mechanical behaviour and properties: A scoping review of current approaches and limitations. *Orthod. Craniofacial Res.* **2022**, *25*, 199–211. [CrossRef] [PubMed]
25. Ceddia, M.; Marchioli, G.; Romasco, T.; Comuzzi, L.; Piattelli, A.; Deporter, D.A.; Di Pietro, N.; Trentadue, B. Effect of Crestal Position on Bone–Implant Stress Interface of Three-Implant Splinted Prostheses: A Finite Element Analysis. *Materials* **2025**, *18*, 3344. [CrossRef] [PubMed]
26. Tan, F.; Wang, C.; Yang, C.; Huang, Y.; Fan, Y. Biomechanical Effects of Various Bone-Implant Interfaces on the Stability of Orthodontic Miniscrews: A Finite Element Study. *J. Health Eng.* **2017**, *2017*, 7495606. [CrossRef] [PubMed]
27. Paul, P.; Mathur, A.K.; Chitra, P. Stress distribution patterns in mini-implant and bone in the infra-zygomatic crest region at different angulations: A finite element study. *J. World Fed. Orthod.* **2021**, *10*, 29–34. [CrossRef]
28. Ramirez-Fernandez, O.; Duran-Gonzalez, I.; Equihua-Guillen, F.; Avila, L.C.; Camporredondo, E.; Garcia-Lara, A.; Zuñiga-Aguilar, E. Design and structural deformation assessment of three-dimensional printed dental implants by means of finite element analysis. *Technol. Health Care* **2025**, 09287329251346282. [CrossRef]
29. Meng, W.-Y.; Ma, Y.-Q.; Shi, B.; Liu, R.-K.; Wang, X.-M. The comparison of biomechanical effects of the conventional and bone-borne palatal expanders on late adolescence with unilateral cleft palate: A 3-dimensional finite element analysis. *BMC Oral Health* **2022**, *22*, 600. [CrossRef]
30. Zhang, S.; Choi, Y.; Li, W.; Shi, D.; Tang, P.; Yang, L.; Wang, Y.; Yang, X.; Wu, J. The effects of cortical bone thickness and miniscrew implant root proximity on the success rate of miniscrew implant: A retrospective study. *Orthod. Craniofacial Res.* **2022**, *25*, 342–350. [CrossRef]

31. Yu, J.-H.; Wang, Y.-T.; Lin, C.-L. Customized surgical template fabrication under biomechanical consideration by integrating CBCT image, CAD system and finite element analysis. *Dent. Mater. J.* **2018**, *37*, 6–14. [CrossRef]
32. Goswami, M.; Sahu, A.; Prasad, R.R.; Priya, P.; Roy, S.; A, A. Comparison of stress distribution and displacement pattern of maxillary expansion in craniomaxillary complex using rapid maxillary expander and maxillary skeletal expander: A finite element model analysis. *Int. Orthod.* **2025**, *23*, 100997. [CrossRef]
33. Olmez, C.; Halicioglu, K.; Gok, G.D.; Koc, O. Optimizing mandibular second molar mesialization: A comparative analysis of stress distribution and displacement using tie-back and temporary skeletal anchorage device-assisted mechanisms with a nonlinear finite element model. *Am. J. Orthod. Dentofac. Orthop.* **2025**, *168*, 451–465. [CrossRef]
34. Vale, F.; Travassos, R.; Couto, I.; Ribeiro, M.; Marques, F.; Caramelo, F.; Marto, C.M.; Spagnuolo, G.; Paula, A.B.; Nunes, C.; et al. Patient's Perspective on Miniscrews During Orthodontic Treatment—A Systematic Review With Meta-Analysis. *Orthod. Craniofacial Res.* **2025**, *28*, 217–241. [CrossRef]
35. Braak, M.C.v.D.; Hoekstra, J.W.M.; Bronkhorst, E.M.; Schols, J.G.; Ongkosuwito, E.M.; Meijer, G.J.; Beucken, J.J.v.D. The effect of surface roughening on the success of orthodontic mini-implants: A systematic review and meta-analysis. *Am. J. Orthod. Dentofac. Orthop.* **2024**, *165*, 262–271. [CrossRef]
36. Katyal, S.; Bhatia, N.K.; Sardana, R.; Singh, S.; Chugh, A.; Shamim, M.A.; Anil, A.; Negi, A.; Chugh, V.K. Success rate and factors affecting stability of infrazygomatic miniscrew implants: A systematic review and meta-analysis. *Eur. J. Orthod.* **2025**, *47*, cjae074. [CrossRef] [PubMed]
37. Valeri, C.; Aloisio, A.; Marzo, G.; Costigliola, G.; Quinzi, V. What is the impact of patient attributes, implant characteristics, surgical techniques, and placement location on the success of orthodontic mini-implants in young adults? A Systematic Review and Meta-Analysis. *Saudi Dent. J.* **2024**, *36*, 1149–1159. [CrossRef]
38. Romanec, C.L.; Panaite, T.; Zetu, I.N. Dimensions Define Stability: Insertion Torque of Orthodontic Mini-Implants: A Comparative In Vitro Study. *J. Clin. Med.* **2025**, *14*, 1752. [CrossRef]
39. Moga, R.A.; Olteanu, C.D.; Botez, M.; Buru, S.M. Assessment of the Maximum Amount of Orthodontic Force for Dental Pulp and Apical Neuro-Vascular Bundle in Intact and Reduced Periodontium on Bicuspids (Part II). *Int. J. Environ. Res. Public Health* **2023**, *20*, 1179. [CrossRef]
40. Sarika, K.; Kumaran, N.K.; Seralathan, S.; Sathishkumar, R.K.; Preethi, S.K. A Three-dimensional finite element analysis of the stress distribution around the bone mini-implant interface based on the mini-implant angle of insertion, diameter, and length. *J. Pharm. Bioallied Sci.* **2023**, *15*, S535–S539. [CrossRef]
41. Lim, J.; Lee, S.; Kim, Y.; Lim, W.; Chun, Y. Comparison of cortical bone thickness and root proximity at maxillary and mandibular interradicular sites for orthodontic mini-implant placement. *Orthod. Craniofacial Res.* **2009**, *12*, 299–304. [CrossRef]
42. Melsen, B.; Agerbæk, N.; Markenstam, G. Intrusion of incisors in adult patients with marginal bone loss. *Am. J. Orthod. Dentofac. Orthop.* **1989**, *96*, 232–241. [CrossRef]
43. Van Steenbergen, E.; Burstone, C.J.; Prahl-Andersen, B.; Aartman, I.H.A. The influence of force magnitude on intrusion of the maxillary segment. *Angle Orthod.* **2005**, *75*, 723–729. [CrossRef]
44. Pedersen, E.; Isidor, F.; Gjessing, P.; Andersen, K. Location of centres of resistance for maxillary anterior teeth measured on human autopsy material. *Eur. J. Orthod.* **1991**, *13*, 452–458. [CrossRef]
45. Bulcke, M.M.V.; Dermaut, L.R.; Sachdeva, R.C.; Burstone, C.J. The center of resistance of anterior teeth during intrusion using the laser reflection technique and holographic interferometry. *Am. J. Orthod. Dentofac. Orthop.* **1986**, *90*, 211–220. [CrossRef]
46. Coolidge, E.D. The Thickness of the Human Periodontal Membrane. *J. Am. Dent. Assoc. Dent. Cosm.* **1937**, *24*, 1260–1270. [CrossRef]
47. Baumgaertel, S.; Hans, M.G. Buccal cortical bone thickness for mini-implant placement. *Am. J. Orthod. Dentofac. Orthop.* **2009**, *136*, 230–235. [CrossRef] [PubMed]
48. Arantes, V.d.O.R.; Corrêa, C.B.; Lunardi, N.; Neto, R.J.B.; Spin-Neto, R.; Boeck, E.M. Insertion angle of orthodontic mini-implants and their biomechanical performance: Finite element analysis. *Rev. Odontol. UNESP* **2015**, *44*, 273–279. [CrossRef]
49. Seo, J.-H.; Kim, M.-S.; Lee, J.-H.; Eghan-Acquah, E.; Jeong, Y.-H.; Hong, M.-H.; Kim, B.; Lee, S.-J. Biomechanical efficacy and effectiveness of orthodontic treatment with transparent aligners in mild crowding dentition—A finite element analysis. *Materials* **2022**, *15*, 3118. [CrossRef]
50. Khaohoen, A.; Sornsuwan, T.; Chaijareenont, P.; Poovarodom, P.; Rungsiyakull, C.; Rungsiyakull, P. Biomaterials and clinical application of dental implants in relation to bone density—A narrative review. *J. Clin. Med.* **2023**, *12*, 6924. [CrossRef]
51. Agustine, C.; Soegiharto, B.M. Stress Distribution of Anterior Tooth Apex and Their Surrounding Alveolar Bone during Maxillary Anterior Intrusion on Segmented and Continuous Wires (3D Finite Element Analysis). *J. Int. Dent. Med. Res.* **2018**, *11*, 596–601.
52. Wu, J.; Wang, X.; Jiang, Y.; Wu, Z.; Shen, Q.; Chen, Y.; Meng, Q.; Ye, N. Effect of archwire plane and archwire size on anterior teeth movement in sliding mechanics in customized labial orthodontics: A 3D finite element study. *BMC Oral Health* **2022**, *22*, 33. [CrossRef]

53. Chu, C.; Chung, C.; Lin, P.; Wang, S. Fabrication of porous NiTi shape memory alloy for hard tissue implants by combustion synthesis. *Mater. Sci. Eng. A* **2004**, *366*, 114–119. [CrossRef]
54. Yu, J.-H.; Lin, Y.-S.; Chang, W.-J.; Chang, Y.-Z.; Lin, C.-L. Mechanical effects of micro-thread orthodontic mini-screw design on artificial cortical bone. *J. Med. Biol. Eng.* **2014**, *34*, 49–55. [CrossRef]
55. Balamurali, V.; Magesh, V.; Harikrishnan, P. Effect of cortical bone thickness on shear stress and force in orthodontic miniscrew-bone interface—A finite element analysis. *Biomed. Phys. Eng. Express* **2024**, *10*, 55013. [CrossRef]
56. Su, R.; Sun, J.; Li, S.; Wang, W. Biomechanical effects of aligner trimline design and intrusion protocol on mandibular anterior teeth: A finite element study. *BMC Oral Health* **2025**, *25*, 1798. [CrossRef]
57. Mazhari, M.; Khanehmasjedi, M.; Mazhary, M.; Atashkar, N.; Rakhshan, V. Dynamics, Efficacies, and Adverse Effects of Maxillary Full-Arch Intrusion Using Temporary Anchorage Devices (Miniscrews): A Finite Element Analysis. *BioMed Res. Int.* **2022**, *2022*, 6706392. [CrossRef]
58. Vadvadgi, V.; Bhardwaj, A.; Padmawar, S.S.; Belludi, A. Study of stress distribution in maxillary anterior region during true intrusion of maxillary incisors using finite element methodology. *Int. J. Exp. Dent. Sci.* **2014**, *1*, 89–92. [CrossRef]
59. Ghorab, H.; Ramadan, A.A.F.; Nadim, M.A.; Sharaf, T. Finite element study to evaluate the stress around mini-implant during canine retraction using continuous and interrupted orthodontic forces. *Open Access Maced. J. Med. Sci.* **2023**, *11*, 36–43. [CrossRef]
60. Hirai, Y.; Watanabe, K.; Deguchi, T.; Ueda, K.; Hamada, K.; Tanaka, E. Influence of insertion depth on stress distribution in orthodontic miniscrew and the surrounding bone by finite element analysis. *Dent. Mater. J.* **2021**, *40*, 1270–1276. [CrossRef] [PubMed]
61. Şavkan, İ.; Marşan, G.; Tağrikuu, B. Three-dimensional finite element analysis of the effects of different force vectors on tooth movement in miniscrew-assisted en masse retraction. *Eur. Oral Res.* **2025**, *59*, 179–185. [CrossRef] [PubMed]
62. Liu, T.-C.; Chang, C.-H.; Wong, T.-Y.; Liu, J.-K. Finite element analysis of miniscrew implants used for orthodontic anchorage. *Am. J. Orthod. Dentofac. Orthop.* **2012**, *141*, 468–476. [CrossRef]
63. Zrinski, M.T.; Pavlic, A.; Katic, V.; Spalj, S. Effect of personality traits on the association between clinically assessed malocclusion and the psychosocial impact of dental aesthetics. *Orthod. Craniofacial Res.* **2023**, *26*, 62–71. [CrossRef]
64. Singh, J.R.; Kambalyal, P.; Jain, M.; Khandelwal, P. Revolution in Orthodontics: Finite element analysis. *J. Int. Soc. Prev. Community Dent.* **2016**, *6*, 110–114. [CrossRef]
65. Sakamaki, T.; Watanabe, K.; Iwasa, A.; Deguchi, T.; Horiuchi, S.; Tanaka, E. Thread shape, cortical bone thickness, and magnitude and distribution of stress caused by the loading of orthodontic miniscrews: Finite element analysis. *Sci. Rep.* **2022**, *12*, 12367. [CrossRef]
66. Guo, R.; Lam, X.Y.; Zhang, L.; Li, W.; Lin, Y. Biomechanical analysis of miniscrew-assisted molar distalization with clear aligners: A three-dimensional finite element study. *Eur. J. Orthod.* **2024**, *46*, cjad077. [CrossRef]
67. Kuc, A.E.; Sybilski, K.; Kotuła, J.; Piątkowski, G.; Kowala, B.; Lis, J.; Saternus, S.; Sarul, M. The hydrostatic pressure distribution in the periodontal ligament and the risk of root resorption—A finite element method (fem) study on the nonlinear innovative model. *Materials* **2024**, *17*, 1661. [CrossRef]
68. Bharadwaj, A.; Ahuja, S.; Uppal, J.; Bhambri, E.; Sewta, R.; Gupta, S. A 3D finite element analysis of biomechanical effects on teeth and bone during true intrusion of anteriors using miniscrews. *Int. Orthod.* **2025**, *23*, 100925. [CrossRef]
69. Yadav, S.; Chen, J.; Upadhyay, M.; Jiang, F.; Roberts, W.E. Comparison of the force systems of 3 appliances on palatally impacted canines. *Am. J. Orthod. Dentofac. Orthop.* **2011**, *139*, 206–213. [CrossRef]
70. Tepedino, M.; Chimenti, C.; Masedu, F.; Potrubacz, M.I. Predictable method to deliver physiologic force for extrusion of palatally impacted maxillary canines. *Am. J. Orthod. Dentofac. Orthop.* **2018**, *153*, 195–203. [CrossRef]
71. Akbulut, Y.; Ozdemir, S. Optimizing Miniscrew Stability: A Finite Element Study of Titanium Screw Insertion Angles. *Biomimetics* **2025**, *10*, 650. [CrossRef]
72. Jasmine, M.I.F.; Yezdani, A.A.; Tajir, F.; Venu, R.M. Analysis of stress in bone and microimplants during en-masse retraction of maxillary and mandibular anterior teeth with different insertion angulations: A 3-dimensional finite element analysis study. *Am. J. Orthod. Dentofac. Orthop.* **2012**, *141*, 71–80. [CrossRef]
73. Noble, J.; Karaiskos, N.E.; Hassard, T.H.; Hechter, F.J.; Wiltshire, W.A. Stress on bone from placement and removal of orthodontic miniscrews at different angulations. *J. Clin. Orthod.* **2009**, *43*, 332–334. [PubMed]
74. Auwer, O.N.; Shamaa, M.S.; Hammad, S.M. A 3-dimensional finite element analysis to evaluate the impact of force direction, insertion angle, and cortical bone thickness on mini-screw and its surrounding bone. *J. Dent. Res. Dent. Clin. Dent. Prospect.* **2021**, *15*, 262–268. [CrossRef] [PubMed]

75. Grzeskowiak, R.M.; Schumacher, J.; Dhar, M.S.; Harper, D.P.; Mulon, P.-Y.; Anderson, D.E. Bone and cartilage interfaces with orthopedic implants: A literature review. *Front. Surg.* **2020**, *7*, 601244. [CrossRef]
76. Kohli, N.; Stoddart, J.C.; van Arkel, R.J. The limit of tolerable micromotion for implant osseointegration: A systematic review. *Sci. Rep.* **2021**, *11*, 10797. [CrossRef]